

Uncertainty Quantification Metrics for Deep regression

Simon Kristoffersson Lind^{a,1,*}, Ziliang Xiong^{b,1}, Per-Erik Forssén^b, Volker Krüger^a

^a{firstname}.{lastname}@cs.lth.se, Lund University LTH, Lund, Sweden

^b{firstname}.{lastname}@liu.se, Linköping University, Linköping, Sweden

Abstract

When deploying deep neural networks on robots or other physical systems, the learned model should reliably quantify predictive uncertainty. A reliable uncertainty allows downstream modules to reason about the safety of its actions. In this work, we address metrics for uncertainty quantification. Specifically, we focus on regression tasks, and investigate Area Under Sparsification Error (AUSE), Calibration Error (CE), Spearman’s Rank Correlation, and Negative Log-Likelihood (NLL). Using synthetic regression datasets, we look into how those metrics behave under four typical types of uncertainty, their stability regarding the size of the test set, and reveal their strengths and weaknesses. Our results indicate that Calibration Error is the most stable and interpretable metric, but AUSE and NLL also have their respective use cases. We discourage the usage of Spearman’s Rank Correlation for evaluating uncertainties and recommend replacing it with AUSE.

1. Introduction

In recent years, there has been a rapid advance in the adoption of neural network-based methods for many tasks in robotics. Following this adoption, increasing scrutiny has been directed towards neural network-based methods for their lack of reliability and interpretability. While neural networks have achieved impressive performance for many different tasks, the fact remains that they can be unreliable in real-world deployment (Grimmett et al., 2016). Additionally, their lack of interpretability makes it difficult to know how and when they may perform unreliably. For these reasons, increasing attention has been directed at the uncertainty output from neural networks, and the importance of introspective qualities (Grimmett et al., 2016). Arguably the most important introspective quality is a reliable uncertainty estimate.

Despite increasing attention being directed toward *uncertainty quantification* (UQ), most of the work is directed toward uncertainty in classification tasks. In robotics, regression problems are common, and there is a lack of common understanding surrounding the available metrics. In this work, we have identified four metrics that are commonly used to measure various qualities in a predicted uncertainty in regression. Specifically, we investigate the *Area Under Sparsification Error* (AUSE) (Ilg et al., 2018), *Spearman’s Rank Correlation* (Spearman, 1904), *Negative Log Likelihood* (NLL) (Lakshminarayanan et al., 2017), and *Calibration Error* (CE) (Pakdaman Naeini et al., 2015). These UQ metrics measure different aspects of uncertainty that are all orthogonal to the regression task performance (typically *mean squared*

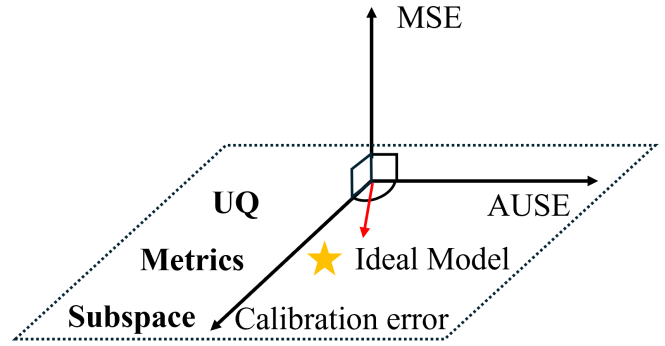


Figure 1: An illustration for UQ metrics and regression metrics. Note: the axes of CE and AUSE are distinct, but not orthogonal.

error (MSE)) as indicated in Fig. 1.

With the help of synthetic datasets, we explore the usage of these metrics with the aim of understanding exactly what they measure, their limitations and whether or not their measurements are useful for practical applications.

Our contributions are as follows:

- We create simple synthetic datasets that highlight different types of uncertainty, and use these to explore how the metrics behave, compared to the generating data distribution.
- We compare each metric in terms of their stability to different dataset sizes.
- Finally, we reason about the strengths and limitations of each metric.

Additionally, we provide a mathematical formulation for the AUSE metric. To the best of our knowledge, AUSE has previously only been described informally, using natural language.

*Corresponding author:

Email address: simon.kristoffersson_lind@cs.lth.se (Simon Kristoffersson Lind)

¹Equal contribution

2. Related Work

Historically, methods that deal with any type of uncertainty in regression have been formulated using parameterized distributions. As a classic example, consider Kalman filters (Kalman, 1960), which are built on a parameterized distribution with well-defined uncertainty. Modern machine learning methods are built upon a solid statistical foundation and most methods output some form of uncertainty (Bishop, 2006). However, it has been observed that there is a discrepancy between the predicted uncertainty from modern neural networks, and the observed empirical accuracy (Guo et al., 2017). Additionally, lacking interpretability in these uncertainties have led to the development of methods to formulate more statistically grounded uncertainties (Gawlikowski et al., 2023).

Along with the research on uncertainty estimation, a number of methods have been developed to assess how trustworthy a predicted uncertainty is. Perhaps the most commonly used (for example in Guo et al. (2017); Kuleshov et al. (2018)) is the *expected calibration error* (ECE) (Pakdaman Naeini et al., 2015). While not as common as ECE, NLL (*negative log likelihood*) is also used, for example in Heiss et al. (2022); Loquercio et al. (2020). Spearman’s rank correlation coefficient (Spearman, 1904) has also found new use in this area (for example in Tan et al. (2023); Ng et al. (2023)). Finally, the most recent method we examine is AUSE (Ilg et al., 2018), used in for example Eldesokey et al. (2020); Xiong et al. (2024). While other uncertainty assessment methods exist, we have chosen to focus on these four as they are most commonly used.

3. Theory

First, we introduce different types of uncertainty in Sec. 3.1. Then, in Sec. 3.2, we introduce the four common uncertainty evaluation metrics to be analyzed.

3.1. Different types of Uncertainty

In the realm of predictive uncertainty estimation, we encounter two fundamental types of uncertainty (Kendall & Gal, 2017). The first, known as *aleatoric uncertainty*, encompasses the intrinsic noise and ambiguity present in observations. This noise, stemming from sources like sensor or motion irregularities, persists even with an increase in data collection and cannot be mitigated. The second type, *epistemic uncertainty* constitutes the uncertainty surrounding model parameters, reflecting our lack of knowledge about the precise model generating the observed data. This form of uncertainty tends to diminish as more data is acquired, and is thus often termed *model uncertainty*. The most common cause of epistemic uncertainty is *out-of-distribution* (OOD) data. In other words, data that comes from a distribution that is different from the training data. For example, autonomous driving models that are trained on synthetic data usually face domain gap to real-world data.

Aleatoric uncertainty can be subdivided into *homoscedastic uncertainty*, which remains constant across various inputs, and *heteroscedastic uncertainty*, which varies depending on the model inputs. Heteroscedastic uncertainty plays a crucial role in computer vision tasks. For example, in depth regression, images with intricate textures and prominent vanishing lines typically yield confident predictions, whereas images of featureless surfaces are expected to produce higher uncertainty.

3.2. Uncertainty Evaluation Metrics

Here, we introduce the four selected uncertainty metrics for the deep regression tasks. We define the metrics as functions of a dataset $S = \{(\mathbf{x}_i, y_i) \mid i = 1, 2, \dots, N\}$, consisting of input-output pairs (\mathbf{x}_i, y_i) . For any learned model, we further define $F(\mathbf{x}; \theta) \mapsto \mathbb{R}$, and $U(\mathbf{x}; \theta) \mapsto \mathbb{R}$ to be functions based on the model parameters θ . $F(\mathbf{x}; \theta)$ produces a prediction of y , and $U(\mathbf{x}; \theta)$ produces an uncertainty estimate.

AUSE: *Sparsification plots* are widely used in optical flow (Mac Aodha et al., 2013; Wannewetsch et al., 2017) and stereo disparity (Häger et al., 2021) to assess how well the predicted uncertainty coincides with the prediction error on a test dataset. Ilg et al. (2018) define AUSE in natural language for the comparison among approaches with different main task performances. Here we present a formal mathematical definition.

AUSE is computed as an aggregate metric over a dataset S consisting of input-output (\mathbf{x}_i, y_i) pairs. We define the *mean absolute error* (MAE) on S as:

$$\text{MAE}(S) = \frac{1}{|S|} \sum_{(\mathbf{x}_i, y_i) \in S} |y_i - F(\mathbf{x}_i; \theta)| . \quad (1)$$

Based on a parameter $\alpha \in [0, 1]$, we partition S into disjoint subsets $S_{\wedge}(\alpha)$ and $S_{\vee}(\alpha)$ such that $|S_{\wedge}(\alpha)| = \alpha|S|$, and

$$\begin{aligned} |y_i - F(\mathbf{x}_i; \theta)| &\geq |y_j - F(\mathbf{x}_j; \theta)| \\ \forall (\mathbf{x}_i, y_i) \in S_{\wedge}(\alpha), (\mathbf{x}_j, y_j) \in S_{\vee}(\alpha) . \end{aligned} \quad (2)$$

In other words, the size of $S_{\wedge}(\alpha)$ is a fraction α of the entire set S , and all absolute errors in $S_{\wedge}(\alpha)$ are larger than those in $S_{\vee}(\alpha)$. We also define analogous partitions $S_{\wedge}^U(\alpha)$ and $S_{\vee}^U(\alpha)$ with respect to the uncertainty:

$$\begin{aligned} U(\mathbf{x}_i; \theta) &\geq U(\mathbf{x}_j; \theta) \\ \forall (\mathbf{x}_i, y_i) \in S_{\wedge}^U(\alpha), (\mathbf{x}_j, y_j) \in S_{\vee}^U(\alpha) . \end{aligned} \quad (3)$$

With these partitions in place, we define:

$$\text{AUSE}(S) = \int_0^1 \frac{\text{MAE}(S_{\vee}^U(\alpha))}{\text{MAE}(S)} - \frac{\text{MAE}(S_{\vee}(\alpha))}{\text{MAE}(S)} d\alpha . \quad (4)$$

AUSE computes the normalized area between the two curves $\text{MAE}(S_{\vee}^U(\alpha))$ and $\text{MAE}(S_{\vee}(\alpha))$ formed by varying α from 0 to 1. The curve $\text{MAE}(S_{\vee}(\alpha))$ is called the *oracle*, which represents a lower bound on sparsification. In practice, the integral (4) is replaced with summing over finite test set samples. See Fig. 5 for an example.

Calibration Error The reliability diagram (Niculescu-Mizil & Caruana, 2005) and the expected calibration error (Pakdaman Naeni et al., 2015) are originally diagnostic tools for classification models that compare sample accuracy against predicted confidence. However, this approach does not apply to regression tasks. Therefore, Kuleshov et al. (2018) introduce a calibration plot for regression tasks in terms of the cumulative distribution function from the model, and summarize it with CE as a numerical score. Formally, let the predicted probability distribution of an input \mathbf{x}_i be $P(y_i|\theta) = F(\mathbf{x}_i; \theta)$. The empirical frequency is then defined as

$$\hat{p}_j = \frac{|\{y_i \mid P(y < y_i|\theta) \leq p_j, (\mathbf{x}_i, y_i) \in S\}|}{N} . \quad (5)$$

Here $p_j \in [0, 1]$ represents an arbitrary threshold value. Given M distinct thresholds p_1, p_2, \dots, p_m (typically evenly spaced from 0 to 1), the calibration error is defined for regression as

$$\text{cal}(\hat{p}_1, \dots, \hat{p}_N) = \sum_{j=1}^M w_j (p_j - \hat{p}_j)^2 , \quad (6)$$

where w_j are arbitrary scaling weights, usually $w_j = \frac{1}{N|\hat{p}_j|}$.

Spearman correlation In 1904, psychologist Charles Spearman defined what he called the *rank method* of correlation (Spearman, 1904). He observed that there may exist correlations that would not be adequately captured by simple linear correlation. Instead, he argued that more complex correlations may be adequately captured by comparing *ranks* of elements.

Given a set of samples, the rank of a sample is simply the index that number would have in a list. More formally, let $L = [x_1, x_2, \dots, x_N]$ be a sequence of samples, then the rank of a sample is defined as:

$$r(x_i) = 1 + |\{x_j \mid x_j < x_i, x_j \in L\}| . \quad (7)$$

We then define the rank operation for a sequence:

$$R(L) = [r(x_1), r(x_2), \dots, r(x_N)] . \quad (8)$$

Spearman’s rank method is then the correlation between two rank sequences:

$$\rho_{R(L_1), R(L_2)} = \frac{\text{cov}(R(L_1), R(L_2))}{\sigma_{R(L_1)} \sigma_{R(L_2)}} . \quad (9)$$

When used as a metric for uncertainty, this correlation is computed between the predictive uncertainty, and the absolute prediction errors.

NLL The popular negative log-likelihood is proved to be a *strictly proper scoring rule* (Lakshminarayanan et al., 2017). Given a dataset $S = \{(\mathbf{x}_i, y_i) \mid i = 1, 2, \dots, N\}$ and a probability density function $p(y|\mathbf{x})$ parameterised by learnable parameters θ , the NLL is defined as

$$\text{NLL}(S) = - \sum_{i=1}^N \log p(y_i|\mathbf{x}_i; \theta) . \quad (10)$$

In expectation, the NLL is minimized if and only if $p(y_i | \mathbf{x}_i; \theta)$ is equal to the true underlying data distribution (Hastie et al., 2009). As such, the NLL can also be used as a metric for uncertainty predictions, since a model with a lower NLL does a better job (in expectation) of fitting the true data distribution.

3.3. Regression Models with Uncertainty Predictions

There exist many different model architectures that incorporate uncertainty predictions. Note that our goal is not to investigate properties in the models. We choose to only use two different models, namely an ensemble and an energy-based model.

3.3.1. Deep Ensemble (DE)

Ensemble learning combines the predictions from multiple individual models to achieve better predictive performance than any single model. For estimating predictive uncertainty, *Deep Ensemble* (DE) (Lakshminarayanan et al., 2017) is a simple yet effective method that trains multiple models in the same architecture with different random initialization and data shuffling. The ensemble is treated as a uniformly weighted mixture model. In practice, for the regression task, each individual model outputs two scalars, which are interpreted as the mean and variance of a Gaussian distribution, and then it is trained to minimize the Gaussian NLL loss as in (11) on the training set.

$$-\log p_\theta(y_n | \mathbf{x}_n) = \frac{\log \sigma_\theta^2(\mathbf{x})}{2} + \frac{(y - \mu_\theta(\mathbf{x}))^2}{2\sigma_\theta^2(\mathbf{x})} + C \quad (11)$$

We follow the suggestion by Lakshminarayanan et al. (2017) to train 5 models and thus get a mixture of Gaussians. This mixture is further approximated by a Gaussian whose mean and variance are the mean and variance of the mixture respectively.

3.3.2. Energy Based Regression (EBR)

Energy-based learning involves learning an energy function $\mathcal{E}(x)$. The goal when learning $\mathcal{E}(x)$ is to assign low energy to observed samples (Gustafsson et al., 2019). Learning $\mathcal{E}(x)$ is in many ways analogous to learning a probability density function, and as such, it has commonly been used for unsupervised learning tasks (Gustafsson et al., 2019). Gustafsson et al. (2019) construct a supervised regression model based on an energy function. First, they define $f_\theta(x, y) \mapsto \mathbb{R}$ to be their learned energy function. Then, they construct a probability density function:

$$p(y|\mathbf{x}; \theta) = \frac{e^{f_\theta(\mathbf{x}, y; \theta)}}{Z(\mathbf{x}; \theta)}, \quad Z(\mathbf{x}; \theta) = \int e^{f_\theta(\mathbf{x}, \tilde{y}; \theta)} d\tilde{y} . \quad (12)$$

Parameters θ are trained by minimizing the NLL with respect to the training data:

$$\mathcal{L} = - \frac{1}{N} \sum_{i=1}^N \log Z(x_i; \theta) - f(x_i, y_i; \theta) . \quad (13)$$

$Z(x_i; \theta)$ is approximated by Monte Carlo sampling. Predictions are generated by performing multi-start gradient ascent to maximize $f(x_i, \tilde{y}; \theta)$ with respect to \tilde{y} .

4. Experiments and Results

4.1. Synthetic Regression Datasets

In order to gauge the behavior of the different uncertainty metrics, we construct four simple synthetic regression datasets, each with a different source of uncertainty. These can be seen in Fig. 2. We will henceforth refer to these datasets by their names: *homoscedastic*, *heteroscedastic*, *multimodal*, and *epistemic*. The names homoscedastic and heteroscedastic are in reference to the type of Gaussian noise applied to the generating function. Multimodal refers to the fact that data is generated from two separate generating functions. Finally, epistemic, refers to the epistemic uncertainty arising from a gap in the training data. Fundamentally, each dataset is a collection of input-output pairs (x, y) . Outputs y are generated as follows:

- Homoscedastic:

$$y = \cos(1.5\pi x) + \epsilon, \quad \epsilon \sim \mathcal{N}(0, 0.1) .$$
- Heteroscedastic:

$$y = \cos(1.5\pi x) + \epsilon, \quad \epsilon \sim \mathcal{N}(0, 0.4 \cdot |\cos(1.5\pi x)|) .$$
- Multimodal:

$$y = 0.5 \pm \cos(2\pi x) + \epsilon, \quad \epsilon \sim \mathcal{N}(0, 0.05) .$$
- Epistemic:

$$y = 0.5 + \cos(4\pi x) + \epsilon, \quad \epsilon \sim \mathcal{N}(0, 0.05) .$$

Here, $\mathcal{N}(0, \sigma)$ refers to a Gaussian distribution with mean 0, and standard deviation σ . \pm in the definition of the multimodal dataset refers to a equal chance of being + or -, which represents the two different modes. In the epistemic dataset, there is a gap in the training data for $x \in [0.35, 0.65]$, which is not present in the test data. This means test data is OOD, which causes epistemic uncertainty. Domains for the inputs are $x \in [-1, 1]$ for the homoscedastic and heteroscedastic datasets, and $x \in [0, 1]$ for the multimodal and epistemic datasets.

4.2. Implementation Details

For each synthetic dataset, we train one EBR model, and one DE model. Both types of models were trained with a batch size of 128 using the Adam (Kingma & Ba, 2015) optimizer. Fig. 3 shows the resulting log-likelihood functions from the models, along with their predictions on our test sets.

Energy Based Regression We implement EBR as a 9-layer perceptron with ReLU activations and a hidden size of 256, which we train for 20 epochs with a fixed learning rate 10^{-4} .

Deep Ensemble All models in our ensemble are identical 5-layer perceptrons, with ReLU activations, and a hidden size of 256. We train each model for 20 epochs with a fixed learning rate of 10^{-3} . In our experiments we use the predicted variance as $U(x)$, more choices are compared by Xiong et al. (2024).

4.3. Stability on varying test set sizes

All metrics are estimates that are computed on a test set of finite size. It is thus important to investigate how quickly each metric converges to its expected value, and whether the estimates are biased for small test set sizes.

First, in order to test convergence, we emulate a process of iteratively collecting points. We begin with generating a single large test dataset of size 2^{16} . From this dataset, we randomly sample data points without replacement, which allows us to investigate how the approximation of each metric behaves as the number of data points increases. We evaluate each metric at test set sizes $2^3, 2^4, \dots, 2^{16}$. The resulting metrics from each subset are reported in Fig. 4 (a).

Second, in order to investigate any bias in the approximation of each metric, we sample 100 i.i.d. datasets at each size $2^3, 2^4, \dots, 2^{16}$. We then report the average of each metric over these 100 datasets in Fig. 4 (b). If a metric is truly unbiased, the average at a small dataset size should converge to the same value as the average at larger dataset sizes.

For both experiments, we use our heteroscedastic dataset because we believe it is the best candidate to highlight any stability issues, due to its varying noise levels.

4.4. Metrics under different types of uncertainty

We compute all metrics for both our models on the test sets of each of the four datasets. As a reference, we compare the results to those computed on the data-generating distribution. Using the data generating distribution will, in expectation, minimize NLL and CE, and should provide a good point of comparison for all metrics. We summarize metrics of both models for each dataset in Tab. 1, 2, 3 and 4 respectively.

Table 1: Metrics for all models on Homoscedastic dataset.

	AUSE↓	CE↓	NLL↓
DE	0.5915	0.0023	-0.8819
EBR	0.5707	0.0032	-0.8568
True dist.	0.5917	0.0003	-0.8965

Table 2: Metrics for both models on Heteroscedastic dataset.

	AUSE↓	CE↓	NLL↓
DE	0.2334	0.0001	-0.1091
EBR	0.2422	0.0001	-0.0990
True dist.	0.2305	0.0001	-0.1472

Table 3: Metrics for both models on multimodal dataset.

	AUSE↓	CE↓	NLL↓
DE	0.0071	0.0229	0.8098
EBR	0.5821	0.0018	-0.6535
True dist.	0.5180	0.0001	-0.7935

Table 4: Metrics for both models on epistemic dataset.

	AUSE↓	CE↓	NLL↓
DE	0.6016	0.0145	36.4332
EBR	1.3888	0.0298	31.2425
True dist.	0.5454	0.0001	-1.5871

5. Discussion

Here we analyze the experiment results, and reason about various strengths and limitations of each metric.

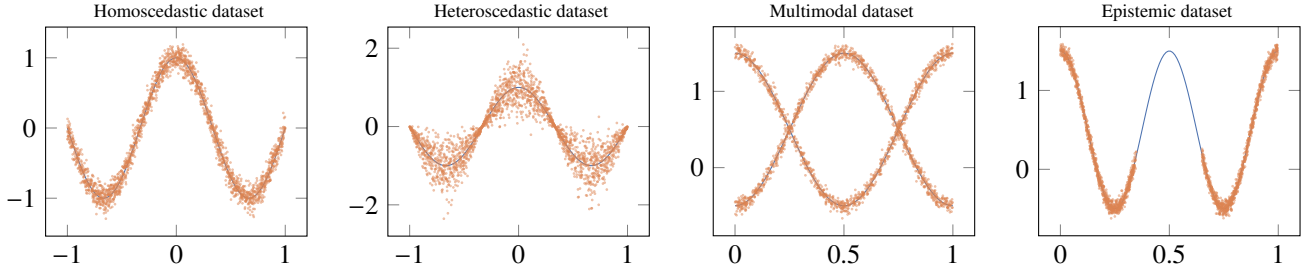


Figure 2: The four synthetic regression datasets. Data points are orange, and the solid blue lines represent the expectation of the generating function.

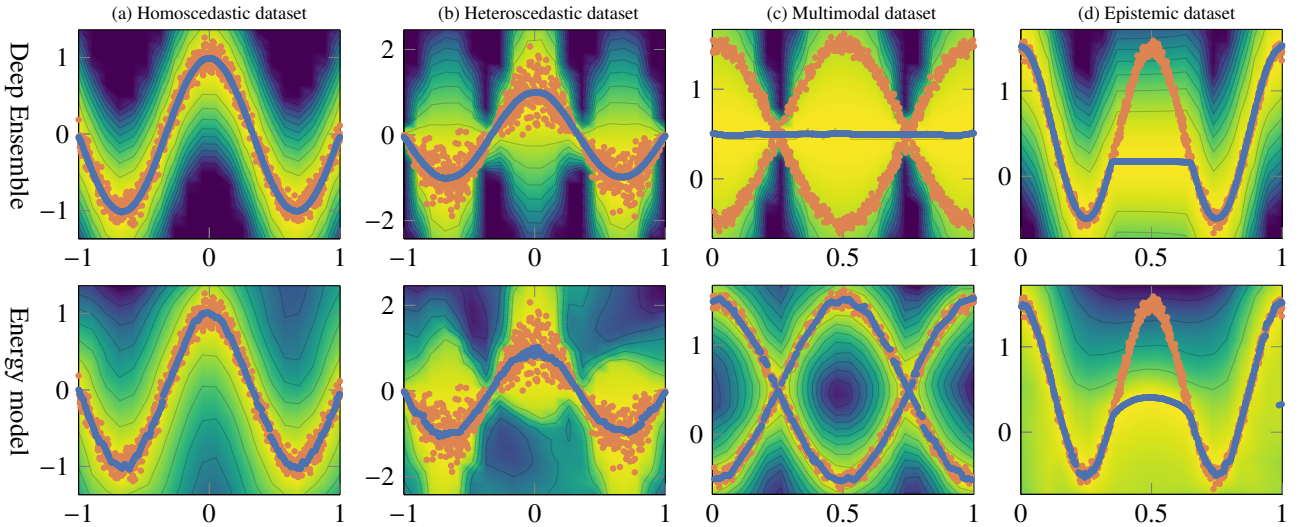


Figure 3: Visualization of the predicted density on the test set for trained models. Contour plots: Log-likelihood output from each model. Yellow: the high-density region; Blue: the low-density region. Blue points: Predicted mean. Orange points: Test set.

5.1. Stability on varying test set sizes

From Fig. 4 (a) we can see that all metrics vary as the test set sizes increase and finally converge to the expectation. We can conclude that all metrics converge beyond a dataset size of 2^{10} . Hence, for most modern regression applications, where test datasets are larger than ~ 1000 samples, stability should not be a cause for concern. Though the amplitudes of metrics vary from each other, arguably we can also conclude that CE is the most stable and AUSE converges second fastest.

From Fig. 4 (b) we can see that the averages change for different dataset sizes. We will henceforth refer to this behavior as *estimation bias of mean*. Arguably, estimation bias is undesirable, since we expect the average of a metric to converge to the same value regardless of the dataset size. As such, a metric with significant bias of the mean should be considered unstable and its use discouraged. Overall, CE is the most stable and AUSE the second most in terms of bias of the mean. We can also conclude that no metric seems to exhibit any meaningful bias beyond a dataset size of 2^6 . Nevertheless, there is still visible bias with dataset size 2^5 , where the total number of samples collected in 100 test sets is much larger than the previously suggested size 2^{10} . This indicates that it is better to collect one large test set than to aggregating many smaller test sets.

Together, these two plots suggest that the most stable met-

ric is CE, followed by AUSE, then NLL, and finally Spearman correlation. Surprisingly, in both Fig. 4 (a) and (b), Spearman correlation has a large value with small test set sizes and gradually converges to zero as the test set size grows. This can be explained by a closer look at Fig. 3 (b): All points close to $x = 0$ will have similar predicted uncertainty values, but their errors may be vastly different, which counteracts the correlation between error and uncertainty. Naturally, this counteracting effect becomes less impactful when samples are sparse. By extension, it is also less impactful in higher-dimensional spaces, and Spearman correlation has been used successfully on for example the rMD17 dataset (Christensen, 2020).

5.2. Metrics under different types of uncertainty

Results for Spearman correlation will not be displayed in the following experiments as it converges to zero.

Homoscedastic and Heteroscedastic datasets: In Fig. 3 (a) and (b) we can see that both models learn predictive distributions close to the generating functions (defined in Sec. 4.1).

In Tab. 1 and 2, all metrics suggest that both models learn the homoscedastic and heteroscedastic distributions approximately equally well. In Fig. 5 (a), the sparsification curve is nearly horizontal, indicating that it is impossible to learn a meaningful correlation between errors and uncertainty. The

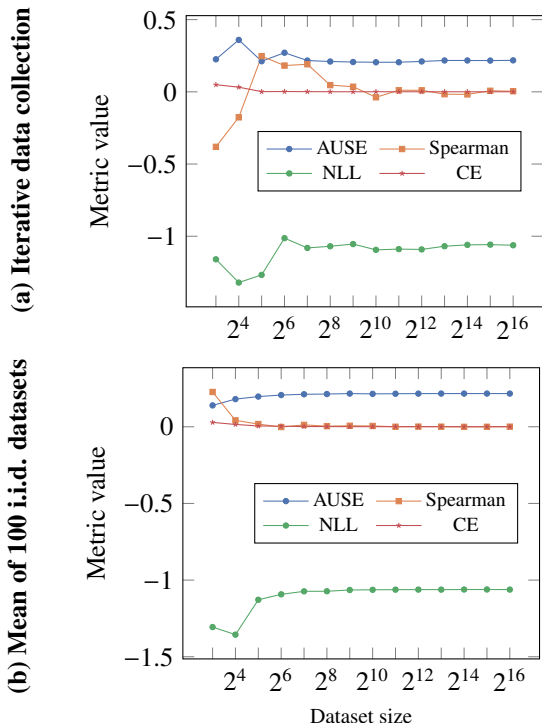


Figure 4: Experiments to test two types of stability of metrics under different test dataset sizes.

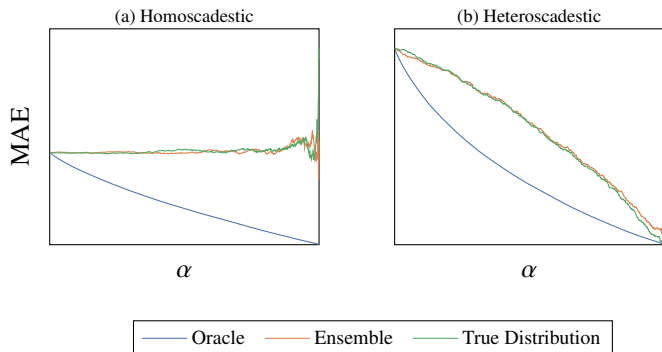


Figure 5: Sparsification plot from Deep Ensemble and True Distribution for the homoscedastic and heteroscedastic datasets. α is the fraction of removed samples.

predicted variance can only partially explain the error, the remaining part is caused by the difference between the annotation and the predicted mean. Intuitively, we expect this scenario of a perfectly uniform variance to be rare in real-world applications. This also indicates that generating uncertainty measures from the predicted parametric distribution may not be the optimal approach for sorting samples. Fig. 3 (a) and Fig. 5 (b) together further show this: even when the predictive and generating distributions are very well aligned, the AUSE value is not 0. For the heteroscedastic dataset, the true distribution achieves the best NLL, and the DE model is slightly better than EBR model. This is because the DE model learns a sharper distribution than EBR, as can be seen in the contour plots of Fig. 3 (a). NLL, as a proper scoring rule, addresses calibration and sharpness simultaneously (Gneiting & Raftery, 2007).

Multimodal dataset: In Fig. 3 (c) we can see that energy-based model successfully learns to predict both modes, but as the ensemble is not designed to output multimodal predictions, it predicts the average of the modes, and a wide distribution.

Tab. 3 shows larger discrepancy between metrics. All metrics suggest that the energy-based model has learned a good distribution that is close to the generating distribution. AUSE for DE is near perfect, which indicates good detection of when DE fails to predict multiple modes. CE and NLL instead indicate the ensemble’s failure to learn both modes with high values. This highlights the main difference between AUSE (and Spearman correlation) and CE/NLL: AUSE measures a correlation between uncertainty and the absolute error, while CE and NLL measure how well the learned distribution captures the data. This raises the question of which type of measurement is most useful, which we will discuss in Sec. 5.4.

Epistemic dataset: In Fig. 3 (d), both models exhibit somewhat larger uncertainty in the OOD region. However, neither model predicts a distribution that assigns high probability to the test data. Visually, the predicted distributions of both models look similar. The only obvious perceptible difference is the slight bend in the center of the distribution of the EBR model.

In Tab. 4, AUSE indicates that the ensemble predicts distribution that can find OOD samples almost as well as the generating distribution, while the distribution from the EBR model is much worse. Both CE and NLL agree that both models failed to learn a good distribution, but they disagree on which model is worse. The contours in Fig. 3 (d) also shows the DE model gives sharper distribution. It is worth noting that there is an entire field of study of OOD detection, which offers better methods for handling epistemic uncertainty. Here, we are instead interested in whether or not each metric can detect a failure to learn the underlying distribution.

Looking at the AUSE scores of 0.6016 and 1.3888 for the ensemble and EBR models respectively, we can infer that this small bend reduces the correlation between error and uncertainty enough to (more than) double the AUSE score. Intuitively, we would expect these two similar distributions to get similar scores, which is exactly the case with both CE and NLL. This raises questions regarding the stability of AUSE under small model variations.

5.3. Interpretability

CE has well defined bounds which makes it easy to interpret. With NLL and AUSE, this is more difficult. We can compare them across models, however, the lower and upper bounds depend on both model and data.

CE: CE has a lower bound 0 when the predicted and generating distributions are equal. The upper bound, however, is dependent on the number of intervals and the weights w_j .

NLL: The lower bound of NLL is given by the generating distribution, which is typically unknown when training for real-world deployment. The upper bound is positive infinity.

AUSE: From Sec. 5.2 we know that the generating distribution may not even give the optimal lower bound 0. We argue

that predicted variance can only partially explain the error. There is no clear upper bound for AUSE.

In summary, NLL and AUSE can only tell us which model is better at UQ but cannot tell us how good it is. This lack of interpretability constitutes a severe limitation of applying AUSE and NLL into real-world autonomous systems.

5.4. Concluding Remarks

We have tested four common uncertainty assessment metrics on four synthetic datasets that are designed to illustrate properties of these metrics. Below we summarize our conclusions:

Spearman Correlation This metric is in general unsuitable. It has stability issues for small test sets, and converges to zero as the test set size grows, see Sec. 5.1.

AUSE This metric offers a robust quantized measure on the correlation between predictive uncertainty and errors compared with Pearson correlation and Spearman correlation. It tells us how wrong a model prediction is likely to be, which is vital for trust-worthy autonomous systems. On the down side, its value is unbounded and thus it lacks interpretability, and it may fail in tasks where homoscedastic uncertainty dominates (but this is rare in real-world applications). It may be more appropriate for loss prediction (Yoo & Kweon, 2019; Cui et al., 2024), which is another UQ approach compared to predicting full distributions.

Calibration Error This metric has a clear lower bound of 0, and is highly interpretable; It requires the least amount of samples to be stable, and can be extended to general confidence intervals Kuleshov et al. (2018). Limitations are that it requires predicting a distribution, and it does not capture how wrong the predictions can be.

NLL This measures the shape of the predictive distributions, including calibration and sharpness. It fails when the generating distribution is multimodal but the training target is unimodal (Xiong et al., 2024), and it requires the largest amount of test samples to be stable among those tested here.

Essentially CE and NLL measure how well the predicted probability distribution corresponds to the true data generating distribution, but CE is the more interpretable of the two. In contrast, AUSE and Spearman measure how well the predicted uncertainty can tell the magnitude of errors. We discourage the use of Spearman correlation for uncertainty quantification, as AUSE has consistently proved to be more robust. Which metric is deemed most useful will naturally differ between applications.

References

Bishop, C. M. (2006). *Pattern recognition and machine learning*. Information science and statistics. New York: Springer.

Christensen, A., Anders S.; Von Lilienfeld (2020). Revised md17 dataset (rmd17). <https://doi.org/10.6084/m9.figshare.12672038.v3>, .

Cui, P., Zhang, D., Deng, Z., Dong, Y., & Zhu, J. (2024). Learning sample difficulty from pre-trained models for reliable prediction. *Advances in Neural Information Processing Systems*, 36.

Eldesokey, A., Felsberg, M., Holmquist, K., & Persson, M. (2020). Uncertainty-aware CNNs for depth completion: Uncertainty from beginning to end. In *Proceedings of the IEEE/CVF Conference on Computer Vision and Pattern Recognition (CVPR)*.

Gawlikowski, J., Rovile Njjeutcheu Tassi, C., Ali, M., Lee, J., Humt, M., Feng, J., Kruspe, A., Triebel, R., Jung, P., Roscher, R., Shahzad, M., Yang, W., Bamler, R., & Zhu, X. X. (2023). A Survey of Uncertainty in Deep Neural Networks. *Artificial Intelligence Review*, 56, 1513–1589. doi:10.1007/s10462-023-10562-9.

Gneiting, T., & Raftery, A. E. (2007). Strictly proper scoring rules, prediction, and estimation. *Journal of the American statistical Association*, 102, 359–378.

Grimmett, H., Triebel, R., Paul, R., & Posner, I. (2016). Introspective classification for robot perception. *The International Journal of Robotics Research*, 35, 743–762. doi:10.1177/0278364915587924.

Guo, C., Pleiss, G., Sun, Y., & Weinberger, K. Q. (2017). On calibration of modern neural networks. In *International conference on machine learning* (pp. 1321–1330). PMLR.

Gustafsson, F. K., Danelljan, M., Bhat, G., & Schön, T. B. (2019). DCTD: deep conditional target densities for accurate regression. *CoRR, arXiv:1909.12297*.

Hastie, T., Tibshirani, R., & Friedman, J. (2009). *The Elements of Statistical Learning*. Springer Series in Statistics. New York, NY: Springer. doi:10.1007/978-0-387-84858-7.

Heiss, J., Weissteiner, J., Wutte, H., Seuken, S., & Teichmann, J. (2022). NOMU: Neural optimization-based model uncertainty. In *Proceedings of the 39th International Conference on Machine Learning* PLMR 162. doi:10.48550/arXiv.2102.13640.

Häger, G., Persson, M., & Felsberg, M. (2021). Predicting disparity distributions. In *2021 IEEE International Conference on Robotics and Automation (ICRA)* (pp. 4363–4369). doi:10.1109/ICRA48506.2021.9561617.

Ilg, E., Cicek, O., Galesso, S., Klein, A., Makansi, O., Hutter, F., & Brox, T. (2018). Uncertainty estimates and multi-hypotheses networks for optical flow. In *Proceedings of the European Conference on Computer Vision (ECCV)* (pp. 652–667).

Kalman, R. E. (1960). A new approach to linear filtering and prediction problems. *Transactions of the ASME—Journal of Basic Engineering*, 82, 35–45.

- Kendall, A., & Gal, Y. (2017). What uncertainties do we need in bayesian deep learning for computer vision? *Advances in neural information processing systems*, 30.
- Kingma, D., & Ba, J. (2015). Adam: A method for stochastic optimization. In *International Conference on Learning Representations (ICLR)*. San Diego, CA, USA.
- Kuleshov, V., Fenner, N., & Ermon, S. (2018). Accurate uncertainties for deep learning using calibrated regression. In *Proceedings of the 35th International Conference on Machine Learning* (p. 2796–2804). PMLR.
- Lakshminarayanan, B., Pritzel, A., & Blundell, C. (2017). Simple and scalable predictive uncertainty estimation using deep ensembles. *Advances in neural information processing systems*, 30.
- Loquercio, A., Segu, M., & Scaramuzza, D. (2020). A general framework for uncertainty estimation in deep learning. *IEEE Robotics and Automation Letters*, 5, 3153–3160. doi:10.1109/LRA.2020.2974682.
- Mac Aodha, O., Humayun, A., Pollefeys, M., & Brostow, G. J. (2013). Learning a confidence measure for optical flow. *IEEE Transactions on Pattern Analysis and Machine Intelligence*, 35, 1107–1120. doi:10.1109/TPAMI.2012.171.
- Ng, M., Guo, F., Biswas, L., Petersen, S. E., Piechnik, S. K., Neubauer, S., & Wright, G. (2023). Estimating uncertainty in neural networks for cardiac mri segmentation: A benchmark study. *IEEE Transactions on Biomedical Engineering*, 70, 1955–1966. doi:10.1109/TBME.2022.3232730.
- Niculescu-Mizil, A., & Caruana, R. (2005). Predicting good probabilities with supervised learning. In *Proceedings of the 22nd international conference on Machine learning ICML '05* (p. 625–632). New York, NY, USA: Association for Computing Machinery. doi:10.1145/1102351.1102430.
- Pakdaman Naeni, M., Cooper, G., & Hauskrecht, M. (2015). Obtaining well calibrated probabilities using bayesian binning. *Proceedings of the AAAI Conference on Artificial Intelligence*, 29. doi:10.1609/aaai.v29i1.9602.
- Spearman, C. (1904). The proof and measurement of association between two things. *The American Journal of Psychology*, 15, 72–101. doi:10.2307/1412159.
- Tan, A. R., Urata, S., Goldman, S., Dietschreit, J. C. B., & Gómez-Bombarelli, R. (2023). Single-model uncertainty quantification in neural network potentials does not consistently outperform model ensembles. *npj Computational Materials*, 9, 1–11. doi:10.1038/s41524-023-01180-8.
- Wannenwetsch, A. S., Keuper, M., & Roth, S. (2017). Probflow: Joint optical flow and uncertainty estimation. In *2017 IEEE International Conference on Computer Vision (ICCV)* (pp. 1182–1191). doi:10.1109/ICCV.2017.133.
- Xiong, Z., Eldesokey, A., Johnander, J., Wandt, B., & Forssén, P.-E. (2024). Hinge-wasserstein: Mitigating overconfidence in regression by classification. In *IEEE Computer Society Conference on Computer Vision and Pattern Recognition Workshops (CVPRW 2024)*.
- Yoo, D., & Kweon, I. S. (2019). Learning loss for active learning. In *2019 IEEE/CVF Conference on Computer Vision and Pattern Recognition (CVPR)* (pp. 93–102). doi:10.1109/CVPR.2019.00018.